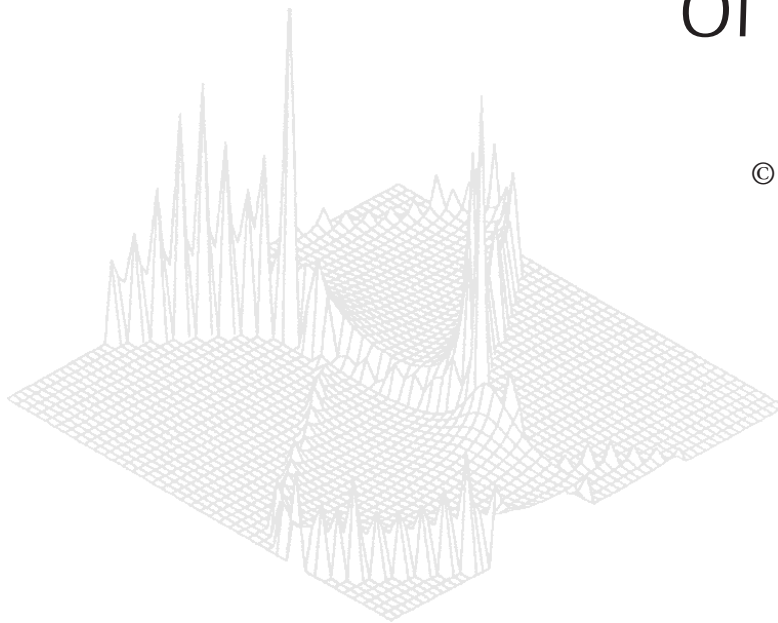

C S I R O P U B L I S H I N G

Australian Journal of Physics

Volume 52, 1999
© CSIRO Australia 1999



A journal for the publication of
original research in all branches of physics

www.publish.csiro.au/journals/ajp

All enquiries and manuscripts should be directed to

Australian Journal of Physics

CSIRO PUBLISHING

PO Box 1139 (150 Oxford St)

Collingwood

Vic. 3066

Australia

Telephone: 61 3 9662 7626

Facsimile: 61 3 9662 7611

Email: peter.robertson@publish.csiro.au



Published by **CSIRO PUBLISHING**
for CSIRO Australia and
the Australian Academy of Science



A Millisecond X-ray Reflectometer

*John W. White,^A Anthony S. Brown,^A Richard F. Garrett,^B David J. King^A
and Trevor L. Dowling^A*

^AResearch School of Chemistry, Australian National University,
Canberra, ACT 0200, Australia.

^BAustralian Nuclear Science and Technology Organisation,
Private Mail Bag 1, Menai, NSW 2234, Australia.

Abstract

Many important processes occur at surfaces and interfaces on timescales ranging from milliseconds up to hours. The advent of third generation synchrotrons provides X-ray fluxes sufficiently high that it is now conceivable that these processes can be studied with millisecond time resolution using X-ray reflectometry. Several configurations for an X-ray reflectometer designed to measure X-ray reflectivity profiles with this time resolution are examined. The feasibility of each configuration in terms of information retrieval from reflectivity data is explored by application of modelling techniques to simulated 'experimental' data.

1. Introduction

It is becoming increasingly apparent that there is a need for a reflectometer to study fast changes in the structure of interfaces, which arise as a response to mechanical, chemical, photochemical and electrochemical actions (Penfold *et al.* 1996; White *et al.* 1996; Hillman *et al.* 1996). For example, neutron reflectometry from polymeric surfactant layers (Saville *et al.* 1994, 1995) has revealed that after a critical surface pressure has been reached in compressing a monolayer film, bilayer, trilayer and multilayer nucleation occurs in response to the mechanical stress. This response occurs in periods of milliseconds to minutes after compression (depending upon the temperature and the chemical nature of the material) and in some cases is viscoelastic. There are also subsequent slow processes, such as hydration of bilayers so formed, and these may take from minutes to hours for completion. It appears evident that high speed reflectometry would give new insights into thin film elasticity and rheology in the time domain 10^{-3} to 10^3 s. This paper investigates the parameters of a novel instrument to meet this need.

The great intensity of X-ray radiation from synchrotron sources and the ultimate possibility of using contrast variation through the anomalous component of the scattering factor, however, indicate that the X-ray method has great potential which might be applied to the resolution of problems for which neutron or X-ray methods are inapplicable or too slow.

2. New Techniques—New Possibilities

Elegant X-ray reflectometers using a single X-ray wavelength (either from an emission line or by use of a suitable monochromator) are now available to measure

the X-ray reflectivity from, for example, the air–water interface, by scanning the incident and reflected angles simultaneously. Perpendicular momentum transfers $Q_z = (4\pi/\lambda)\sin\theta$, where θ is the incident angle and λ the wavelength, between 0.005 and 0.5 \AA^{-1} have been achieved with these instruments and methods of refining the data, either singly or jointly with neutron data (Russell 1990; Foster 1993), have been developed. Such instruments allow the reflectivity profile from a particular interface to be obtained with a real space resolution of a few angstroms.

The type of instrument proposed in the present paper uses the broad wavelength band of X-rays generated either as bremsstrahlung in a laboratory source or as synchrotron radiation from a bending magnet or as harmonics from undulators (see e.g. Gluskin 1996). A broad wavelength band is used to maximise the photon flux on the reflecting surface and to take advantage of the anomalous dispersion for wavelength dependent contrast variation. Various options for such an instrument will be explored here.

In an attempt to get the fastest real time resolution, the reflectivity could, for example, be determined simultaneously at say ten points on the curve at time intervals of about one millisecond provided that a suitably intense beam can be brought to the reflecting surface. The number of points needed to reconstruct the full reflectivity curve to a desired resolution is here analysed using a combination of model fitting programs and equilibrium data taken at much higher resolution for the same system (e.g. before and after application of the stress).

The opportunity to construct and use such an instrument arises now because the intensities of the broad band radiation from third generation synchrotrons are approaching 10^{20} photons sec^{-1} . The opportunity to participate in novel beamline design at these sources, the growing understanding of X-ray and neutron reflectivity as methods for surface profile determination and of recent developments in very fast semiconductor detectors for X-rays (X-ray counting rates up to 10^8 photons sec^{-1}) make a new type of instrument possible. The performance of this instrument is calculated below.

3. Calculations on Model Systems

The viability of an energy-dispersive X-ray reflectometer and the data collection times which could be expected for such an instrument depend upon the flux available at the detector. Each element in the optical path changes the spectral distribution. To estimate the data collection times we have calculated the effects of reflection of the beam by the beam-steering mirror and subsequently by an air–water interface.

For our calculations we have taken the spectral distribution of the APS Wiggler A beamline operating at a current of 100 mA. The flux data are based on a sample positioned 30 m from the source, and a beam dimension of 0.1 mm (vertical) \times 10.0 mm (horizontal). One option to meet the multi-segment approach (below) for an energy-dispersive instrument is to have several standard settings of different angles of incidence onto the sample. This requires several angles of incidence of the synchrotron beam onto the steering mirror. We have calculated the effects of reflection of the beam from a Pt-coated mirror with a surface roughness of 3 \AA , for two representative angles of incidence. For an angle of incidence onto the mirror of 0.25°, the reflected beam has the spectral distribution shown in Fig. 1*a*. Subsequent reflection from a water surface with a

surface roughness of 3 \AA (having a reflectivity typical of the systems of interest here) gives the distribution shown in Fig. 1c. The corresponding distributions for reflection at 0.5° from the Pt mirror and subsequent reflection from water at 1.0° are shown in Figs 1b and 1d. The final count rate at the detector for such a configuration is thus in the range 10 to 10^9 photons sec^{-1} for an angle of incidence of 1.0° on the sample, and 10^5 to 10^{10} photons sec^{-1} for an angle of incidence of 0.5° on the sample. The range of scattering vectors accessible at these angles is 0.044 – 0.265 \AA^{-1} at 0.5° and 0.089 – 0.530 \AA^{-1} at 1.0° .

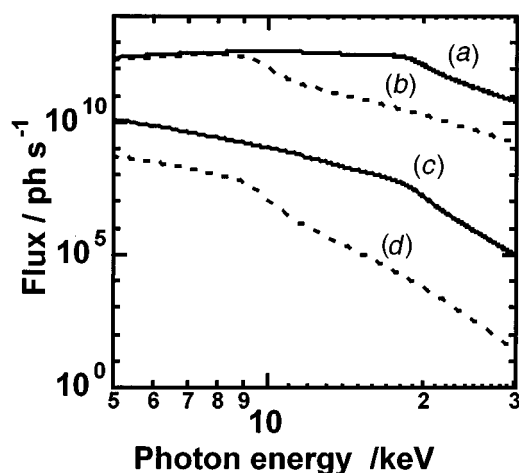


Fig. 1. Flux as a function of energy for the APS Wiggler A (0.1% BW, 1.0 mm^2 spot 30 m from the source and 100 mA current): (a) After Pt steering mirror, $\theta_i = 0.25^\circ$, then (c) after reflection from water at $\theta_i = 0.5^\circ$; (b) after Pt steering mirror, $\theta_i = 0.5^\circ$, then (d) after reflection from water at $\theta_i = 1.0^\circ$.

(3a) Simulated Data

In order to explore the range of applicability of the proposed instrument we have calculated the reflectivity profiles for some model systems. Firstly we explore the extent to which, the statistics at the high Q_z end of the reflectogram can be increased relative to those of a fixed wavelength machine by choosing the best possible spectral distribution for the incident X-ray beam. We have also studied the effects of anomalous dispersion for a simple system containing only one atom type with a significant imaginary component in the scattering factor for the incident wavelength range. As a first model we consider the measurement time and quality of a reflectogram from a cadmium stearate monolayer at the air–water interface. An instrument of the type illustrated in Fig. 8 below is assumed for this analysis. This has variable incident angle and several crystal analysing detectors.

The incident collimation of the synchrotron beam (and hence that of the reflected beam) along with the mosaic spread of the analysing monochromator, determines the energy resolution (and hence the Q_z resolution) of the instrument. Optimisation of the analysing crystals and their arrangement is a key design

component. Fig. 2 shows a superposition (with small vertical offsets) of the reflectograms for a cadmium stearate monolayer at the air–water interface calculated for various incident angles from 0.25° to 1.50° for radiation in the range 5–30 keV (see also Table 1). Data from these different angles can be combined to give a single reflectivity profile as shown in Fig. 3. This also illustrates that

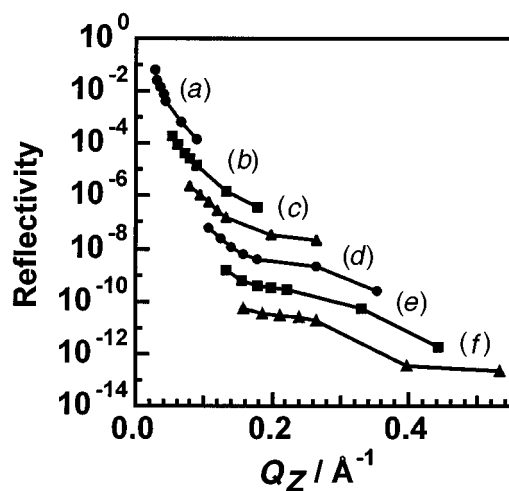


Fig. 2. Energy-dispersive reflectivity profiles for a cadmium stearate monolayer at the air–water interface, neglecting the effects of anomalous dispersion. Each profile was calculated using radiation in the range 6–20 keV (2.067 – 0.62 Å) and a fixed angle of incidence: (a) 0.25° , (b) 0.50° , (c) 0.75° , (d) 1.00° , (e) 1.25° and (f) 1.50° . Profiles (b)–(f) have been successively offset downwards by a factor of 10 for clarity. Appropriately scaled and combined these data produce the profile shown in Fig. 3.

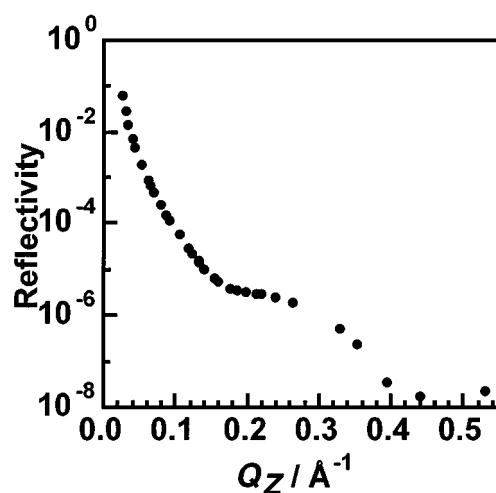


Fig. 3. Reflectivity profile for a cadmium stearate monolayer at the air–water interface. The data in the range $Q_z = 0.089$ – 0.530 Å $^{-1}$ are accessible using 5–30 keV radiation at an angle of incidence of 1.0° . Note that the effect of anomalous dispersion variation as a function of wavelength has not been included in this calculation.

different regions of Q_z space can be easily accessed by suitable choice of the angle of incidence. Optimisation of the signal-to-background of a multiwavelength reflectogram depends on a careful study of the background producing properties (e.g. fluorescence, diffuse scattering) from the different wavelengths.

Table 1. Parameters used in the simulations of cadmium and manganese stearate monolayers at the air–water interface

Densities for Cd, Mn and stearate are based on an area per molecule of 25 \AA^2 for stearate, a length of 23 \AA for stearate and an effective layer thickness of 5 \AA for Cd and Mn. All interface roughnesses were taken to be 3.0 \AA . Here ρ is the scattering length density

	$\bar{\rho} (\times 10^{-6} \text{ \AA}^{-2})$	Physical density (g cm^{-3})
Cd (5 \AA layer)	10.84	1.49
Mn (5 \AA layer)	5.72 (for $\lambda = 0.75 \text{ \AA}$) 3.95 (for $\lambda = 1.895 \text{ \AA}$)	0.73 0.73
Stearate	7.66	0.804
H ₂ O	9.41	1.000

The data immediately illustrate the importance of understanding the sources of background, since measurements down to 10^{-7} of the incident beam are needed to reach a maximum Q_z of 0.5 \AA^{-1} . Equally it is evident that, with the mirror systems described above, a flux on the sample of approximately 10^{12} photons sec^{-1} is needed to make a measurement in one millisecond. Single shot measurements in one second are thus quite feasible and it may be possible to reach a time resolution of 10^{-3} s for long relaxation period systems, e.g. polymer films. One of the objectives mentioned above (i.e. measurement of relaxation spectra in the time domain 10^{-3} to 10^3 s) may thus be realisable.

(3b) Effects of ‘Anomalous’ Dispersion

It will be of the greatest advantage to X-ray reflectometry if the wavelength and magnetic field dependence of X-ray scattering lengths can be used to vary contrast in a way analogous to hydrogen–deuterium contrast variation in neutron scattering. The X-ray method is greatly limited by the number of variables available to the process of getting a unique fit to the observed reflectivity profile, especially for systems with more than one layer. One strategy is to use the models from neutron reflectivity on the same film to fix parameters and follow kinetic phenomena with the X-rays, but it does not seem impossible to get interpretable, wavelength dependent contrast, at least for systems containing only one anomalously dispersive atom type.

A manganese stearate monolayer at the air–water interface represents a system for which the ‘anomalous’ dispersion effect is rather large. The real part of the dispersion correction is -7.514 electrons at a wavelength of 1.895 \AA for manganese. This corresponds to an apparent electron density at the absorption edge which is 30% lower than the true electron density. The real part of the dispersion correction is shown in Fig. 4. Simulated reflectivity profiles for an energy-dispersive instrument are illustrated in Figs 5 and 6. The profile assumes a wavelength spread of $0.5\text{--}2.25 \text{ \AA}$ ($24.8\text{--}5.5 \text{ keV}$) and a fixed angle of incidence of 1.0° . The dispersion correction gives rise to a small peak in the reflectivity at $Q_z = 0.1157 \text{ \AA}^{-1}$. However, the reflectivity differs by at most about 5% from

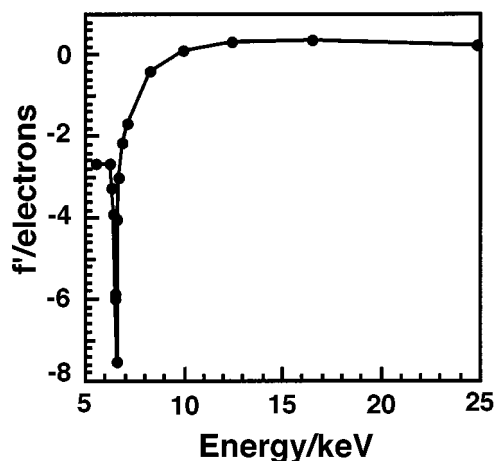


Fig. 4. Dispersion correction for manganese as a function of incident X-ray energy (calculations courtesy of D. C. Creagh).

that in which dispersion effects are neglected (Fig. 6). It is unlikely that such an effect would be detectable experimentally; thus, analysis of data from dispersive systems will be significantly simplified. The Q_z corollary is that dispersion can be used to great effect, if angle-dispersive reflectivity profiles are measured using several different fixed wavelengths, close to and far from the absorption edge. The angle-dispersive reflectivity profiles for manganese stearate are shown in Fig. 7 for comparison with the energy-dispersive profiles in Figs 5 and 6. The reflectivities calculated for incident wavelengths of 0.75 and 1.895 Å differ by as much as 200% (note the logarithmic scale).

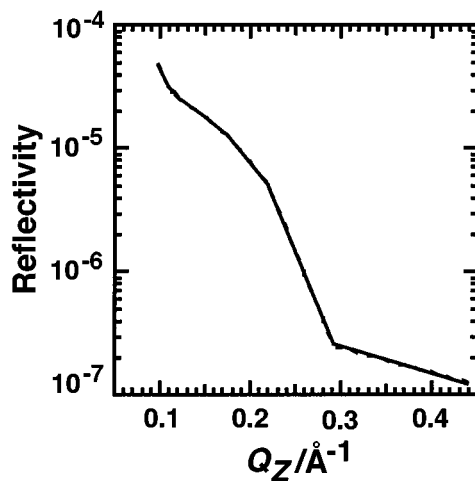


Fig. 5. Energy-dispersive reflectivity profiles for a manganese stearate monolayer at the air-water interface. The solid line is the reflectivity when dispersion is accounted for and the dashed line is for dispersion neglected.

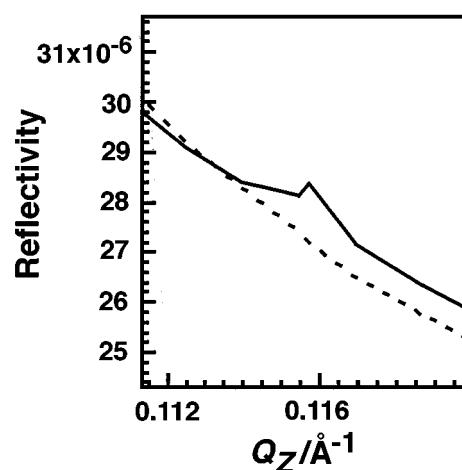


Fig. 6. Detail from Fig. 5, highlighting the reflectivity near the absorption edge for manganese. Note the linear scale.

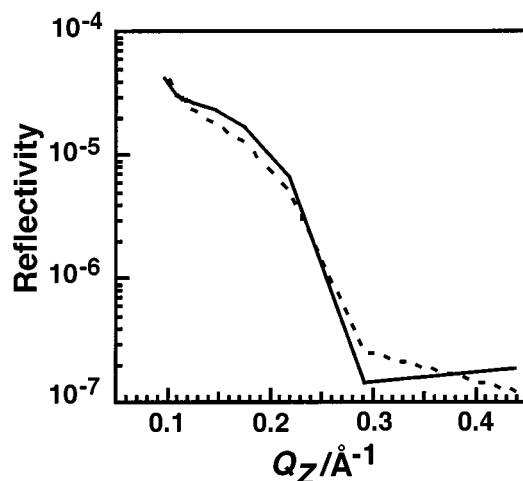


Fig. 7. Angle-dispersive reflectivity profiles at 0.75 \AA (solid line) and 1.896 \AA (dashed line) for a manganese stearate monolayer at the air-water interface. The angular ranges are $0.33\text{--}1.50^\circ$ (solid line) and $0.84\text{--}3.79^\circ$ (dashed line).

4. Instrument Designs

Remembering that surface reflectivity falls off faster than Q_z^{-4} after the critical angle, and that one may wish to measure down to intensity levels of 10^{-7} of the incident beam, it is obvious that a dynamic range of at least 10^8 is required in the detector chain. This is the limit of present avalanche photodiode systems (see e.g. Randall 1996; Toellner *et al.* 1994). To get, say, 10% statistics at the highest Q_z (say 0.5 \AA^{-1}) and to follow interface reorganisation at millisecond time resolution, counting rates up to 10^4 Hz will be needed at this Q_z . The counting rate at the critical angle would then be about 10^{12} Hz. Clearly, measurement of

the specular reflectivity profile at a number of different segments in the space of Q_z is indicated.

Suitable X-ray fluxes are available from third generation synchrotron radiation sources so long as the beam can be brought to the sample without too much loss (e.g. in reflecting mirrors). Fast detection seems possible by using avalanche photodiode systems (Randall 1996; Toellner *et al.* 1994), possibly in combination with other systems. We envisage two classes of detection system, each with several variations of configuration. The first is a fairly conventional energy-dispersive design, the second is a novel ‘crystal-dispersive’ design which makes use of an array of monochromating crystals. Both systems would use the fast counting capabilities and energy resolution characteristics of avalanche photodiodes.

5. Energy Dispersive Detectors

(5a) Conventional Solid State Detectors

The simplest type of energy resolved reflectometer uses a liquid nitrogen cooled, lithium drifted germanium detector for energy analysis of the reflected beam. This is proposed here as one version of the instrument required for the science outlined above, but is limited to counting rates of the order of 15 kHz in the detector and an energy resolution of about 200 eV. This offers a resolution $\Delta Q/Q$ of the order of a few per cent which is more than adequate for studying monolayer films at the air–water interface and the liquid–liquid interface. It is the same as that currently obtainable by advanced neutron reflectometers such as CRISP or SURF at the Rutherford–Appleton Laboratory, the ISIS Neutron Source in the UK (Penfold 1989) and ISIS 95 (1995) (3–9%). The counting rate is too slow, however, for the dynamical studies proposed here. Such an instrument has been constructed by Roser *et al.* (1994) and a similar instrument is operating in prototype on our rotating anode generator at the Research School of Chemistry.

(5b) Avalanche Photodiodes

The avalanche photodiodes currently available have a dynamic range in excess of 10^9 and an energy resolution $\Delta E/E$ of 12% (Radiation Monitoring Services 1994). They can therefore be used as low resolution energy-dispersive detectors in place of more established solid-state detector types. Although the dynamic range of the avalanche photodiode is considerably larger than that of solid-state detectors and the corresponding data acquisition times would be expected to be significantly reduced, the more relaxed resolution suits the study of systems with smoothly varying reflectivity profiles. Those displaying sharply varying features need germanium detectors. The SURF neutron reflectometer, when operated at a resolution of 9%, has about 30 data points in the range $Q_z = 0.05\text{--}0.65 \text{ \AA}^{-1}$, and has produced much useful data on growing interfacial films. In an equivalent X-ray experiment one could expect a higher proportion of the data to contain structural information, since the background for X-ray reflectivity is at least three orders of magnitude less than for neutrons because of the absence of incoherent scattering.

6. Crystal Dispersive Detectors

The favoured instrument proposed here has a multichannel dispersive analyser and an avalanche photodiode array with associated electronic components. This

array, in its static version, has been chosen to have a resolution of about 10% $\Delta Q/Q$ by the appropriate arrangement in real space of the photodiodes. By multichannel operation, counting rates up to 10^8 Hz should be possible in the counting chains but, because the reflectivity falls very quickly in intensity as a function of Q_z , the counting electronics needed at high Q need not be as fast as those needed in the lower Q_z regions.

Apart from speed of measurement, a great advantage of this multiwavelength reflectometer is that the sample, e.g. a liquid surface, need not be disturbed in any way during measurement. Mechanical movements such as those associated with angle-scanning are avoided. The instrument is intended to study phenomena which are modulated by acoustic or other periodic stresses, to be able to 'gate' the data in phase with the modulation etc. and to measure a dynamic response over a fairly wide frequency range (typically 10^3 to 10^{-3} Hz) with noise as low as possible is an important goal.

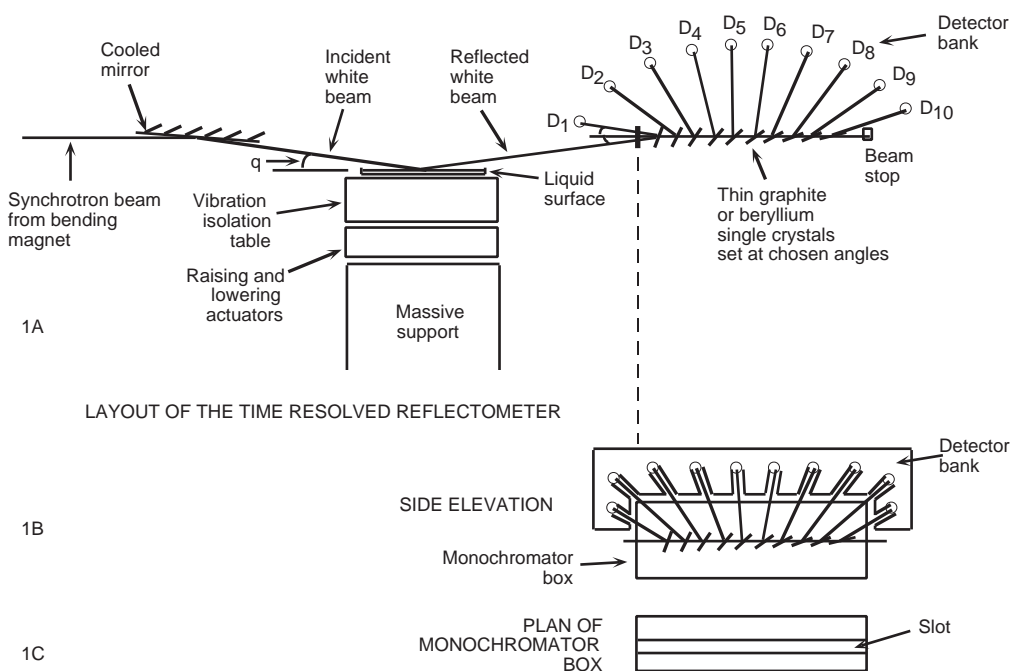


Fig. 8. Layout of the crystal-dispersive multiwavelength reflectometer.

One modification of the energy dispersive device to be used subsequent to X-ray reflection from the interface is a cluster of single crystals arranged in thickness and at angles to the reflected beam direction. The longest wavelength X-rays are reflected from the beam at the front of the array and the more penetrating shorter wavelength radiation reflected from the last crystals into the detector bank. Fig. 8 illustrates this crystal dispersive spectrometer and the reflectivity instrument. In the version shown the crystals are fixed at particular angles to reflect particular wavelengths. In a second version the crystal orientations may be varied by goniometers to 'fill in' the scan.

Beryllium single crystals, the small and almost perfect graphite crystals found in some minerals, small pyrolytic graphite crystals and mica are all suitable crystals for the dispersing device. For a monochromator of relaxed energy resolution and to give a broader band coverage of the reflected beam, synthetic multilayer monochromators or mosaic graphite can be used.

7. Information Content

In previous sections we have shown the feasibility of collecting reflectivity data on a millisecond timescale given the flux available at third generation synchrotron sources and the development of new detector systems. In this section we address the question of information content in reflectivity data, and in particular what instrument resolutions and density of data points are required for useful structural information to be retrieved. In the previous section we considered two basic instrument configurations: energy-dispersive and crystal-dispersive. For the energy-dispersive case the instrument resolution $\Delta Q/Q$ is determined primarily by the energy resolution of the detector, while for the crystal-dispersive case the number and spatial arrangement of monochromator crystals and their mosaic spreads determine the resolution.

Table 2. Parameters used to generate simulated experimental reflectivity data

Parameters common to both models are: all interface roughnesses fixed at 4.0 \AA , a flat background of 2.0×10^{-8} , a resolution $\Delta Q/Q = 3.5\%$, an angle of incidence onto the sample of 1° , and a subphase scattering length density of $9.43 \times 10^{-6} \text{ \AA}^{-2}$

	Model 1	Model 2
d_1 (\AA)	23.0	15.0
$\bar{\rho}_1$ (\AA)	2.5	8.8
d_2 (\AA)	21.0	5.0
$\bar{\rho}_2$ ($\times 10^{-6} \text{ \AA}^{-2}$)	10.3	12.0
d_3 (\AA)	32.0	—
$\bar{\rho}_3$ ($\times 10^{-6} \text{ \AA}^{-2}$)	12.0	—

Simulated ‘experimental’ reflectivity profiles were calculated for two systems with real space dimensions typical of polymeric surfactant systems that we are currently investigating. The models consist of discrete layers of uniform scattering material, and the reflectivity was calculated using the optical transfer matrix method as described by Penfold (1991). The parameters for the two models are given in Table 2. The reflectivity at 825 evenly spaced data points in the range $Q_z = 0.089\text{--}0.50 \text{ \AA}^{-1}$ was calculated assuming an angle of incidence onto the sample of 1° and a $\Delta Q/Q$ of 3.5%, typical of the energy resolution available from a graphite monochromator. This range of scattering vectors is available with energies in the range 5–30 keV for the given angle of incidence. Random fluctuations of 1% were added to simulate experimental noise and measurement errors. Error bars for the data points were calculated assuming a counting time of 1 millisecond, flux at the sample based on the values given in Fig. 1*b*, and a 2% error to account for systematic errors such as may be encountered when placing the data on an absolute scale.

These data sets provide the benchmarks against which the information content of lower resolution data were then judged. Fig. 9 shows the two benchmark data sets. The objective is to see how effectively the starting model can be reproduced by sampling the data of Fig. 9 at an interval typical of the fast instruments proposed above.

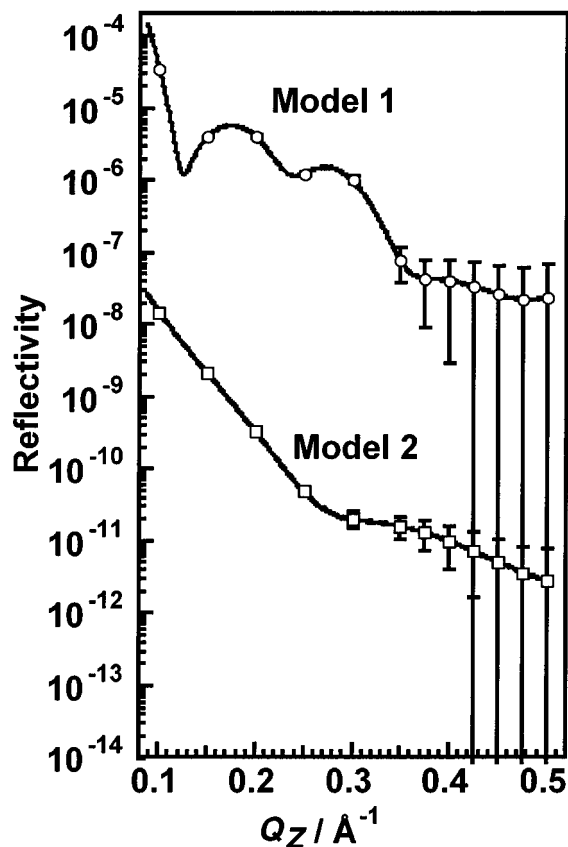


Fig. 9. Benchmark data sets for Model 1 and Model 2. The reflectivity for Model 2 has been offset downwards by a factor of 1000 for clarity. Error bars for only a small subset of the data are shown.

These benchmark data sets were treated in one of two ways to produce data of the type expected from the configurations proposed in this paper:

(1) Data were rebinned at resolutions $\Delta Q/Q$ of 3.5, 5, 10, 15 and 20%, yielding 50, 35, 17, 12 and 9 data points respectively. These profiles were used to evaluate the resolution required in an energy-dispersive design.

(2) Profiles consisting of 11, 16 and 21 data points were constructed by selecting approximately evenly-spaced data points from the benchmark data sets. The crystal-dispersive configuration is essentially a relatively high resolution sampling of data at a small number of points. The profiles were used to evaluate how many such data points are required.

The best least-squares fits to the simulated ‘experimental’ data sets were obtained, again using the optical transfer matrix method. The parameters refined in the fits were the layer thicknesses, scattering length densities and the background. All other parameters were fixed at the values given above. For each model, a standard set of initial estimates for the parameters was used. This was different from that used in the generation of the benchmark data sets but allowed convergence to the correct values when used in the fitting of the benchmark data. That is, it was assumed that in a real situation enough prior knowledge would be available (e.g. from a slow scan of start or end profiles of the process being studied) to avoid convergence to a local (and incorrect) minimum on the least-squares surface.

The data in Fig. 9 show that the error bars due to counting statistics become rather large at scattering vectors greater than 0.35 \AA^{-1} if no binning of data is performed. Even moderate binning consistent with instrument resolution,

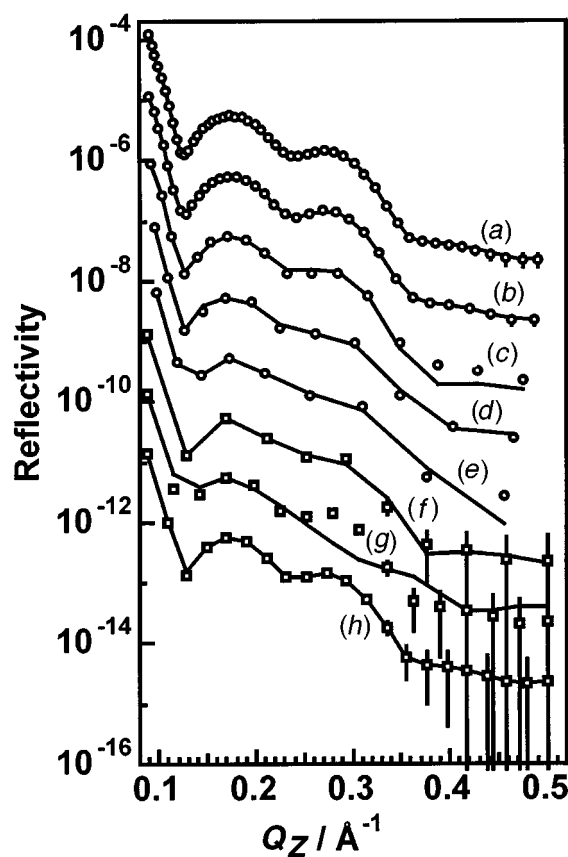


Fig. 10. Model 1 data sets produced from the benchmark data set shown in Fig. 9. Profiles (a)–(e) result from rebinning at $\Delta Q/Q = 3.5, 5.0, 10.0, 15.0$ and 20.0% , respectively, and represent the type of data which would be acquired using an energy-dispersive design. Profiles (f)–(h) result from selection of 11, 16 and 21 data points directly from the benchmark data set, and represent data which would be obtained using the crystal-dispersive design. The solid lines are the best fit to the data in each case.

however, provides data with very much improved counting statistics, as shown in Figs 10 and 11. For example, binning at $\Delta Q/Q = 3.5\%$ gives error bars of 12–30% for data above $Q_z = 0.35 \text{ \AA}^{-1}$ (including the 1% noise and 2% systematic errors).

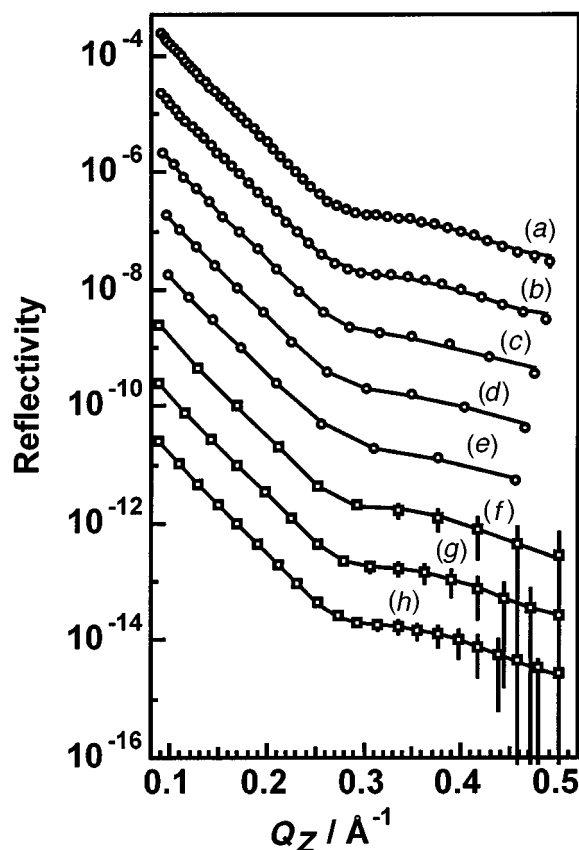


Fig. 11. Model 2 data sets produced from the benchmark data set shown in Fig. 9. Profiles (a)–(e) result from rebinning at $\Delta Q/Q = 3.5, 5.0, 10.0, 15.0$ and 20.0% , respectively, and represent the type of data which would be acquired using an energy-dispersive design. Profiles (f)–(h) result from selection of 11, 16 and 21 data points directly from the benchmark data set, and represent data which would be obtained using the crystal-dispersive design. The solid lines are the best fit to the data in each case.

The reflectivity profile for model 1 is more highly structured and contains higher frequency modulations (Kiessig fringes) than the profile for model 2. This has important consequences when considering which configuration of the reflectometer to adopt, and what density of data points is required to extract useful structural information. The correct structure for model 1 is retrieved from the data which were binned at $\Delta Q/Q = 3.5$ and 5.0% (Figs 10a and 10b), and for 21 data points selected from the benchmark data (Fig. 10h). For model 2 the reflectivity profiles are much less structured and the Kiessig fringes of longer period. The essential features of the structure are retrieved from all of

the profiles shown in Fig. 11, although the uncertainties associated with each of the parameters become larger as the number of data points is reduced. The 5 Å layer in model 2 is not well-resolved in any of the data sets shown in Fig. 11, a consequence of the need for data which extend further in Q_z than is available in the experiment.

The results of this model study indicate that for structures having real space dimensions in the range of approximately 5 to 100 Å, it is desirable that data collected in an energy-dispersive mode should have an energy resolution $\Delta Q/Q$ of between 5 and 10% or better, and for data collected in crystal-dispersive mode the minimum number of data points should be approximately 20. For experiments in which qualitative changes are to be studied as a function of time these requirements could be relaxed.

8. Conclusions

The analysis above suggests that both bending magnet and undulator beam from third generation synchrotron sources have great potential for multiwavelength reflectometry from interfaces. The study of time dependent processes on the millisecond to hour timescale may be possible. Contrast variation using anomalous dispersion (at least for systems with only one anomalous scatterer) is feasible, but is best performed using monochromatic radiation and an angle-dispersive design.

References

- Foster, M. (1993). *Crit. Rev. Anal. Chem.* **24**, 179–241.
- Gluskin, E. (1996). Status of the Insertion Devices, Developments at AP. Presentation by SRI CAT Director to J. Boldeman and J. W. White at APS, 15 January 1996, unpublished.
- Hillman, A. R., *et al.* (1996). ISIS 96. The ISIS Facility Annual Report (Ed. A. D. Taylor), Vol. 2, p. A261.
- ISIS 95 (1995). The ISIS Facility Annual Report (Ed. A. D. Taylor), Vol. 1, pp. 104–5.
- Penfold, J. (1989). *Physica B* **173**, 1–10.
- Penfold, J. (1991). In ‘Neutron, X-ray and Light Scattering’ (Eds P. Lindner and Th. Zemb), p. 223 (Elsevier: Amsterdam).
- Penfold, J., *et al.* (1996). ISIS 96. The ISIS Facility Annual Report (Ed. A. D. Taylor), Vol. 2, p. A270.
- Radiation Monitoring Services (1994). Instruction Manual. Avalanche Photodiode S Series, Watertown, Mass., USA.
- Randall, K. J. (1996). Soft X-ray Instrumentation at the Advanced Photon Source. Presentation to J. Boldeman and J. W. White at APS, 15 January 1996, unpublished.
- Roser, S. J., *et al.* (1994). *Langmuir* **10**, 3853–6.
- Russell, T. P. (1990). *Mater. Sci. Rep.* **5**, 171–271.
- Saville, P. M., *et al.* (1994). *J. Phys. Chem.* **98**, 5935–42.
- Saville, P. M., *et al.* (1995). *J. Phys. Chem.* **99**, 8283–9.
- Toellner, T. S., *et al.* (1994). *Nucl. Instrum. Methods A* **350**, 595–600.
- White, J. W., *et al.* (1996). ISIS 96. The ISIS Facility Annual Report (Ed. A. D. Taylor), Vol. 2, p. A285.